Artificial Intelligence in Agriculture 10 (2023) 26–34

Contents lists available at ScienceDirect

Artificial Intelligence in Agriculture

journal homepage: http://www.keaipublishing.com/en/journals/artificial-intelligence-in-agriculture/

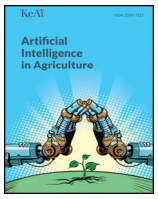

Machine learning-based spectral and spatial analysis of hyper- and multi-spectral leaf images for Dutch elm disease detection and resistance screening

Xing Wei [a], Jinnuo Zhang [a], Anna O. Conrad [b], Charles E. Flower [c], Cornelia C. Pinchot [c], Nancy Hayes-Plazolles [c], Ziling Chen [a], Zhihang Song [a], Songlin Fei [d], Jian Jin [a,*]

[a] Department of Agricultural and Biological Engineering, Purdue University, West Lafayette, IN 47907, United States
[b] USDA Forest Service, Northern Research Station, Hardwood Tree Improvement and Regeneration Center, West Lafayette, IN 47906, United States
[c] USDA Forest Service, Northern Research Station, Delaware, OH 43015, United States
[d] Department of Forestry and Natural Resources, Purdue University, West Lafayette, IN 47907, United States

ARTICLE INFO

Article history:
Received 27 May 2023
Received in revised form 20 September 2023
Accepted 21 September 2023
Available online 26 September 2023

Keywords:
American elm
Dutch elm disease
Hyperspectral imaging
Multispectral imaging
Support vector machine
Convolution neural network
Disease phenotyping
Digital forestry

ABSTRACT

Diseases caused by invasive pathogens are an increasing threat to forest health, and early and accurate disease detection is essential for timely and precision forest management. The recent technological advancements in spectral imaging and artificial intelligence have opened up new possibilities for plant disease detection in both crops and trees. In this study, Dutch elm disease (DED; caused by *Ophiostoma novo-ulmi,*) and American elm (*Ulmus americana*) was used as example pathosystem to evaluate the accuracy of two in-house developed high-precision portable hyper- and multi-spectral leaf imagers combined with machine learning as new tools for forest disease detection. Hyper- and multi-spectral images were collected from leaves of American elm genotypes with varied disease susceptibilities after mock-inoculation and inoculation with *O. novo-ulmi* under greenhouse conditions. Both traditional machine learning and state-of-art deep learning models were built upon derived spectra and directly upon spectral image cubes. Deep learning models that incorporate both spectral and spatial features of high-resolution spectral leaf images have better performance than traditional machine learning models built upon spectral features alone in detecting DED. Edges and symptomatic spots on the leaves were highlighted in the deep learning model as important spatial features to distinguish leaves from inoculated and mock-inoculated trees. In addition, spectral and spatial feature patterns identified in the machine learning-based models were found relative to the DED susceptibility of elm genotypes. Though further studies are needed to assess applications in other pathosystems, hyper- and multi-spectral leaf imagers combined with machine learning show potential as new tools for disease phenotyping in trees.

1. Introduction

Forests play a critical role in our ecosystems by providing various ecological, economic, social, and cultural services (Chen and Meentemeyer, 2016). However, diseases caused by invasive pathogens are an increasing threat to forest health (Flower and Gonzalez-Meler, 2015; Fei et al., 2019). Management options may be limited and prohibitively expensive depending on the extent of pathogen spread and establishment, so early and accurate detection is essential, particularly for invasive pathogens that may not yet be broadly distributed or are cryptic in nature. Current methods for disease detection include observation of visual symptoms, followed by molecular confirmation when needed. However, visual assessment of disease symptoms manually is laborious and prone to errors (Bock et al., 2020; Bian et al., 2022). While early molecular detection methods can generally be developed, they often involve labor-intensive procedures, high costs, and operational limitations (Schaad and Frederick, 2002; Fang and Ramasamy, 2015).

Recent technological advancements have produced new tools, especially spectral imaging combined with artificial intelligence, for rapid and accurate plant phenotyping, including early plant disease detection in both crops and trees (Mishra et al., 2020; Bian et al., 2022). By combining traditional imaging with spectroscopy, spectral imaging can capture both the spatial and spectral features of an object, including healthy and diseased plants, thus enabling the identification of subtle changes associated with disease development before visible symptoms

* Corresponding author at: Department of Agricultural and Biological Engineering, Purdue University, 225 South University Street, West Lafayette, IN 47907, United States.
E-mail address: jinjian@purdue.edu (J. Jin).

https://doi.org/10.1016/j.aiia.2023.09.003

appear (Conrad and Bonello, 2016; Mishra et al., 2020; Singh et al., 2020; Cotrozzi, 2022; Fang et al., 2023). Artificial intelligence has been utilized to analyze complex and high-dimensional data captured by spectral imaging systems. Traditional machine learning methods, such as support vector machine (SVM) and partial least square discriminant analysis (PLS-DA), are commonly used in spectral analysis with satisfactory performance for disease detection in crop and tree systems (Conrad et al., 2020; Wei et al., 2021a; Fearer et al., 2022). State-of-art deep learning models, such as convolution neural networks (CNN), are more suited for image analysis tasks, including spectral image analysis for plant phenotyping and disease detection (Jiang and Li, 2020; Liu and Wang, 2021; Shi et al., 2023). The integration of spectral imaging with machine learning techniques has opened up new possibilities for early detection of plant diseases. However, many major forest diseases remain unexplored by these technological advancements, and additional studies aimed at identifying and detecting disease-specific signatures are needed (Wei et al., 2021b; Cotrozzi, 2022).

Depending on the number of spectral wavelengths/bands involved, spectral imaging can be categorized into hyperspectral imaging (HSI) and multispectral imaging (MSI). Hyperspectral imaging captures and analyzes data across a wide range of narrow spectral bands, which provides a more detailed spectral resolution, thus allowing for the detection of subtle spectral variations associated with plant diseases (Mishra et al., 2017). Multispectral imaging captures data across a limited number of spectral bands, typically ranging from 3 to 10 bands. While it offers less spectral detail compared to HSI, MSI can still provide valuable information for plant disease detection, especially with higher spatial resolutions to capture fine detailed spatial features of disease development (Peng et al., 2022). Both hyper- and multi-spectral imaging techniques have been evaluated for plant disease detection, but mostly in remote sensing systems (Kumar et al., 2012; Chen and Meentemeyer, 2016; Abdulridha et al., 2019; Cotrozzi, 2022). Spectral imaging data collected using remote sensing systems have high throughput but limited imaging resolution, leading to disease detection models primarily relying on averaged canopy color changes (Gitelson and Merzlyak, 1996; Chen and Meentemeyer, 2016). However, early disease symptoms often manifest as small local spots before noticeable canopy color changes occur. In addition, the signal-over-noise ratio (SNR) of remote sensing data is constrained by various sources of noise, including ambient daylight fluctuations, varying leaf slopes, and shadows (Zhang et al., 2019a; Ma et al., 2021). Consequently, the lack of high-SNR imaging sensors capturing high-spectral and spatial resolution disease signals, along with advanced algorithms for accurate disease detection and identification, remains a significant bottleneck in early plant disease diagnosis, including the detection of forest diseases.

The recent development of high-precision leaf spectral imagers, known as LeafSpec, provides high-resolution images in both spectral and spatial domains for accurate plant health monitoring (Zhang et al., 2019b; Wang et al., 2020a, 2020b; Li et al., 2023a, 2023b). The low-cost handheld leaf imaging device was designed to overcome challenges faced by spectral imaging systems, such as inconsistent lighting sources and various leaf slopes, via a customized imaging chamber with embedded light sources and a touch-based scanning mode. The leaf imaging device can collect hyper- or multi-spectral images of a whole leaf directly in the field and in a non-destructive and rapid manner. In addition, LeafSpec has been evaluated with improved performance in detecting nutrient deficiency and discriminating genotypes in both corn and soybean (Wang et al., 2020a, 2020b; Ma et al., 2020; Song et al., 2023). However, most of the previous applications of LeafSpec were in agricultural crop systems, and the high-precision hyper- and multi-spectral leaf imagers have yet to be evaluated in tree phenotyping applications such as disease detection and resistance screening.

In this study, we used Dutch elm disease (DED) in American elm as an example pathosystem to evaluate the capability of LeafSpec for forest disease detection. Dutch elm disease, caused by *Ophiostoma ulmi and O. novo-ulmi,* is one of the most devastating and widespread invasive diseases in U.S. forests (Flower et al., 2017; Fei et al., 2019). The disease was first detected in the first half of the 20th century and has since destroyed American elms (*Ulmus americana*) in urban and forest landscapes across the U.S. (D'Arcy, 2000; Bernier, 2022). Current efforts are focused on identifying and breeding disease-resistant elm trees for use in restoration (Townsend et al., 2005; Pinchot et al., 2017). Therefore, methods capable of rapidly phenotyping trees for disease susceptibility are needed to facilitate these efforts. Past research has demonstrated that Fourier transform-infrared (FT-IR) spectroscopy is sensitive enough to detect changes in elmwood chemistry following infection with *O. novo-ulmi* (Martin et al., 2005a, 2007) and to differentiate between trees that differ in DED susceptibility (Martin et al., 2005b, 2008). However, only xylem tissues of elm trees were destructively examined in the previous studies, and as suggested by the authors, the in-field application of FT-IR for large-scale tree screening is uncertain (Martin et al., 2008). The high-precision handheld LeafSpec shows promise for scaling-up automated in-field plant phenotyping tasks when integrated with robotic systems (Chen et al., 2021, 2023).

The overarching goal of this study is to evaluate the accuracy of high-precision LeafSpec combined with machine learning for disease phenotyping in trees. The specific objectives were to determine 1) if high-resolution spectral images collected using LeafSpec combined with machine learning can detect DED; 2) if there is a different ability using high spectral resolution HSI versus high spatial resolution MSI in detecting DED; 3) can we differentiate elm genotypes with varied susceptibility to DED through machine learning-based analysis of high-resolution leaf images in both spectral and spatial domains.

2. Materials and methods

2.1. Plant material and inoculations

American elm genotypes with known susceptibility to DED were clonally propagated in 2021, potted and grown in a greenhouse at the U.S. Department of Agriculture Forest Service Northern Research Station in Delaware, OH. The experimental unit was one clonal tree in a pot. Trees were organized in a resolvable incomplete block design with three sampling time points, including four elm genotypes and two inoculation treatments, and 4 to 12 replicates per genotype per treatment per sampling time point (Table 1). The four elm genotypes tested included NA 57845, Princeton, RV 141, and RV 467. NA 57845 is an elm clone known for its sensitivity to DED and has been used as a susceptible control in elms breeding programs (Haugen and Bentz, 2017). Princeton is a commercially available American elm clone with high levels of DED tolerance (Townsend et al., 2005; Haugen and Bentz, 2017). The RV 141 and RV 467 genotypes are unique clonal lines developed from seed produced in controlled crosses between known DED-resistant elms. An unpublished field trial has indicated intermediate to low levels of tolerance

Table 1
The number of trees and leaves imaged for each genotype and inoculation treatment.

Elm genotypes	Treatment	96 HPI[a]		4 WPI[b]		15 WPI	
		Trees	Leaves	Trees	Leaves	Trees	Leaves
NA 57845	Mock-inoculated	6	18	7	20	6	21
	Inoculated	10	30	12	24	11	32
Princeton	Mock-inoculated	6	18	5	15	4	26
	Inoculated	10	30	12	24	7	33
RV 141	Mock-inoculated	6	18	6	18	4	19
	Inoculated	10	30	12	24	8	28
RV 467	Mock-inoculated	6	18	6	18	5	24
	Inoculated	10	29	12	24	5	20
Genotype combined	Mock-inoculated	24	58	24	52	19	63
	Inoculated	40	133	48	115	31	140

[a] HPI = hour(s) post inoculation; Leaves imaged at 96 HPI were sampled from a different group of trees as compared to ones in the last two sampling time points.
[b] WPI = week(s) post inoculation; The same group of trees was sampled at 4 and 15 WPI.

for RV 141 clones, and high levels of tolerance for RV 467 clones (C. Flower, personal communication). Two levels of pathogen inoculation treatments were tested, including mock inoculation with water and inoculation with *O. novi-ulmi*. Trees were inoculated following the methods of Pinchot et al. (2017). Briefly, a sterile grafting knife was used to make a small incision that extended into the xylem stream, analogous to a cleft graft, about 10 cm above the base of each potted tree. Either 5 μl of water or fungal spore solution at a concentration of 5×10^3 spores/μl was pipetted into the hole of each tree as the mock-inoculation or inoculation treatment, respectively. The inoculation treatment was applied on May 10 to May 12, 2022.

2.2. Visual disease evaluations

Canopy-level symptoms induced by DED infection, including wilting, yellowing, and browning, were rated as a percent of a tree (using 5% decline ratings) weekly throughout the experiment (Fig. 1C). At the completion of the experiment, which was ~18 weeks post-inoculation (WPI), trees were destructively harvested to confirm pathogen infection via xylem staining. Disease progress curves of each elm genotype were plotted. The visual disease severity rating of DED symptoms before the completion of the experiment (~14 WPI) was compared among elm genotypes using a one-way Analysis of Variance (ANOVA) followed by Tukey honestly significant difference (HSD; $\alpha = 0.05$) to evaluate differences in disease severity ratings among elm genotypes.

2.3. Spectral image collection

Hyper- and multi-spectral leaf images were collected utilizing LeafSpec at three sampling time points, including 96 h post inoculation (HPI; before any visible foliar symptoms of DED developed), 4 WPI (during early foliar symptom development) and 15 WPI (near the conclusion of the experiment when foliage symptoms were visibly noticeable). Fifteen to thirty-three leaves per treatment were imaged for each elm genotype at each sampling time point (Table 1). Trees were destructively sampled for a different study at 96 HPI. Thus, leaves imaged at 96 HPI were from a different group of trees compared to ones at 4 and 15 WPI. Regardless of inoculation treatment, leaves sampled at the first two sampling time points (96 HPI and 4 WPI) did not show any obvious foliar symptoms of DED (asymptomatic). While leaves sampled from the inoculated treatment at 15 WPI had visible DED symptoms, including necrotic leaf tips or yellowing (Fig. 1C). A detached leaf method was used for the image scans, where leaves were detached from each tree and imaged with both hyper- and multi-spectral LeafSpec imagers (Fig. 1A, B). The configuration of these two devices is listed in Table 2. Due to logistical constraints, leaves sampled at 96 HPI and 4 WPI were first stored on wet ice and imaged 6 and 24 h after leaves were detached from trees. In comparison, leaves were imaged immediately after detachment at 15 WPI. A total of 561 leaves were scanned for the three sampling time points, resulting in 561 hyperspectral and 561 multispectral image cube data files, respectively.

2.4. Analysis of hyper- and multi-spectral image cubes

The flow chart for the analysis of hyper- and multi-spectral LeafSpec images is illustrated in Fig. 2. Briefly, raw hyper- and multi-spectral LeafSpec images were first calibrated with a reference image of a flat strip made of white Reflon materials (Wang et al., 2020a). Then, leaf regions in each image were segmented from the background using a threshold method based on normalized difference vegetation index (NDVI) heatmaps derived from the calibrated image cubes (Ma et al., 2020; Song et al., 2023). Traditional machine learning methods, including SVM and PLS-DA, were used for the spectrum analysis. While state-of-art deep learning models, ResNet18, were used for the spectral cube image analysis. Data (either spectra or cube images) for each elm genotype were split into training (70% data) and testing (30% data) subsets using the same random seed to evaluate the training and testing classification accuracies of each machine learning-based model for the

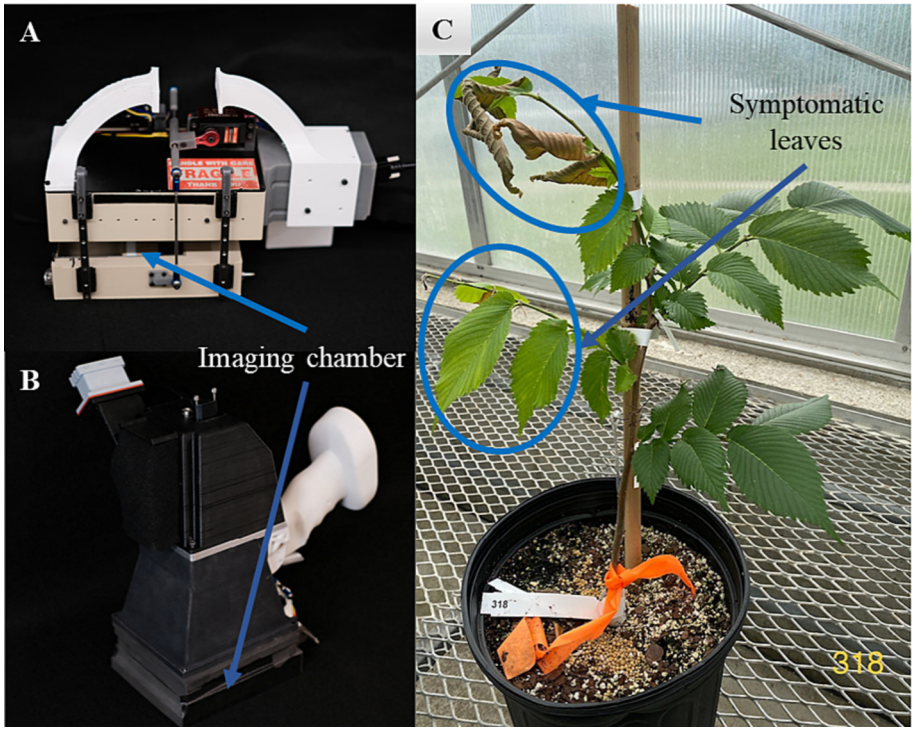

Fig. 1. Handheld LeafSpec: (A) the hyperspectral leaf imager; and (B) the multispectral leaf imager. (C) A potted elm tree showing foliar symptoms of Dutch elm disease (DED) ~4 weeks post-inoculation with *Ophiostoma novo-ulmi*, the causal agent of DED.

Table 2
Configurations of hyper- and multi-spectral LeafSpec imaging devices.

Configurations	Hyperspectral LeafSpec imager	Multispectral LeafSpec imager
Mechanism	Push-broom	Snapshot
Embedded light source	Halogen lights	LED panel
Number of wavebands	368	6
Spectral range	446 to 929 nm	400, 473, 560, 595, 660, 880 nm
Spectral resolution	1 to 2 nm	–
Spatial resolution	~0.5 mm/pixel	~0.04 mm/pixel

detection of DED. The detailed analysis procedures of hyper- and multi-spectral LeafSpec images were described in the following subsections.

2.4.1. Analysis of averaged spectra derived from hyper- and multi-spectral image cubes

The averaged spectrum of a leaf sample was calculated by averaging the spectrums of all the pixels in the leaf regions. The preprocessing steps of averaged spectra derived from hyperspectral image cubes were adapted from Wei et al. (2021a). First, wavelengths at two extreme ends (<490 nm and >900 nm) were removed. Then, spectra were smoothed using a Savitzky-Golay filter with a second-order polynomial and a window size of 11 data points. Lastly, the number of features was reduced by half to 156 wavelengths/bands using a self-developed spectral binning function. In comparison, averaged spectra derived from the 6-band multispectral image were directly used for further analysis.

To classify the mock-inoculated and DED-inoculated treatments, two commonly used supervised machine learning models were tested on the averaged spectra derived from hyper- and multi-spectral LeafSpec images, including linear support vector machine (SVM) and partial least square discriminant analysis (PLS-DA). The linear kernel in SVM finds a linear separator (hyperplane) that maximizes the margin between classes with the least error (Cortes and Vapnik, 1995). PLS-DA aims to find a latent space representation that maximizes the separation between classes. It can handle multicollinearity in spectral data and capture the relevant variation for classification (Chevallier et al., 2006). The hyperparameters for SVM and PLS-DA models were fine-toned using grid search and 10-fold cross-validation. The hyperparameters for each model were selected according to the best training classification accuracy. The range of penalty parameter C in the SVM models was set from 0.001 to 1000 on a logarithmic scale between 10^{-3} and 10^{3} in order to maximize the margin for better classification results and minimize the misclassification errors and overfitting concerns. The range of the number of latent variables for PLS-DA models was set from 2 to 5 for similar reasons. The detailed hyperparameters for each machine learning-based model used in this study were listed in Table S1. SVM and PLSDA models were built using the SVM and PLSRegression packages, respectively. Both packages are in the scikit-learn library in Python (Pedregosa et al., 2011).

2.4.2. Direct analysis of hyper- and multi-spectral cube images using pre-trained CNN models

To make full use of the spectral and spatial features in hyper- and multi-spectral images, pre-trained convolutional neural network (CNN) models, ResNet18, were built and fine-tuned to classify leaves collected from mock-inoculated and inoculated elm trees. ResNet models reformulate the layers as learning residual functions with reference to the layer inputs, which facilitates the training of substantially deeper networks (He et al., 2016). ResNet18, with its deep layers and skip connections, may have the potential to effectively capture complex spatial and spectral features from leaf-level spectral images. During preprocessing, spectral images at two extreme ends (<490 nm and >900 nm) were removed, and neighbor images were binned together using a window size of 5 to reduce multilinearity. The first band image of 560 nm in the multispectral image at 15 WPI was abandoned as an outlier after visual checking of all image bands. After preprocessing, 62-band image cubes were used as input to build the hyperspectral ResNet18 models for all three sampling time points. For the multispectral ResNet18 models, 6-band image cubes were used as input for 96 HPI and 4 WPI, and 5-band image cubes were used for 15 WPI. The adaptive moment estimation algorithm, known as the Adam optimizer, was chosen to iterate the cross-entropy loss function with a learning rate of 0.001. A total of 200 epochs were executed while using a callback function to record the best performance of the trained ResNet18 models. The ResNet-18 model architecture was built using the PyTorch library in Python (Paszke et al., 2019).

2.4.3. Visualization of spectral and spatial feature patterns in DED detection models

To better interpret classification models built upon machine learning algorithms, spectral and spatial feature importance patterns were plotted for the best-performing SVM models built upon averaged spectra derived from hyperspectral images and the ResNet18 CNN model built upon multispectral images, respectively. In the linear SVM models, spectral feature importance was measured by coefficients, representing the weights assigned to each predictor variable in the linear combination that was used to make predictions. In the ResNet18 CNN model built upon multispectral cube images, the class-specific feature heatmaps were generated using Gradient-weighted Class Activation Mapping (Grad-CAM) (Selvaraju et al., 2017). The highlighted regions in each Grad-CAM heatmap represent relatively important features for the model's prediction, which might indicate symptomatic leaves in the current study.

3. Results and discussion

3.1. Visual ratings of foliar symptoms induced by DED infection

The development of foliar symptoms potentially induced by DED after inoculation varied among elm genotypes (Fig. 3). Foliar symptoms such as wilting were observed as early as 2 WPI. However, among four elm genotypes, only NA 57845 had an average rating of over 20% throughout the experiment. A decrease in visual ratings of DED severity occurred from 6 to 9 WPI (Fig. 3A) in tandem with a second flush of vegetative growth in epicormic branches and basal sprouts (data not shown). At 14 WPI, NA 57845 had the greatest DED severity ratings among all four elm genotypes ($P < 0.0001$), numerically followed by RV 141, Princeton, and RV 467 (Fig. 3B). The visual assessment of DED

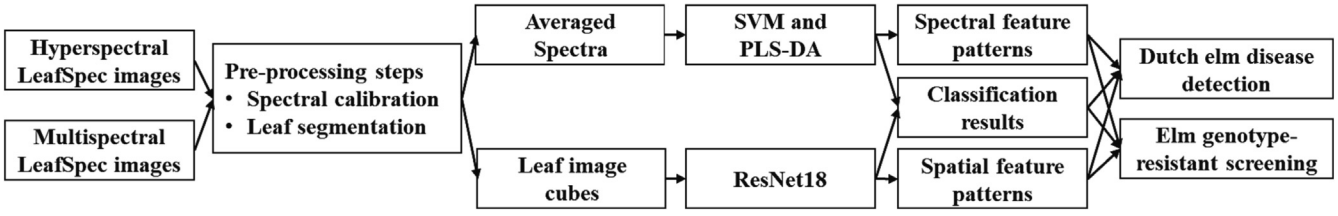

Fig. 2. The flow chart of hyper- and multi-spectral LeafSpec image analysis for Dutch elm disease detection and resistant screening.

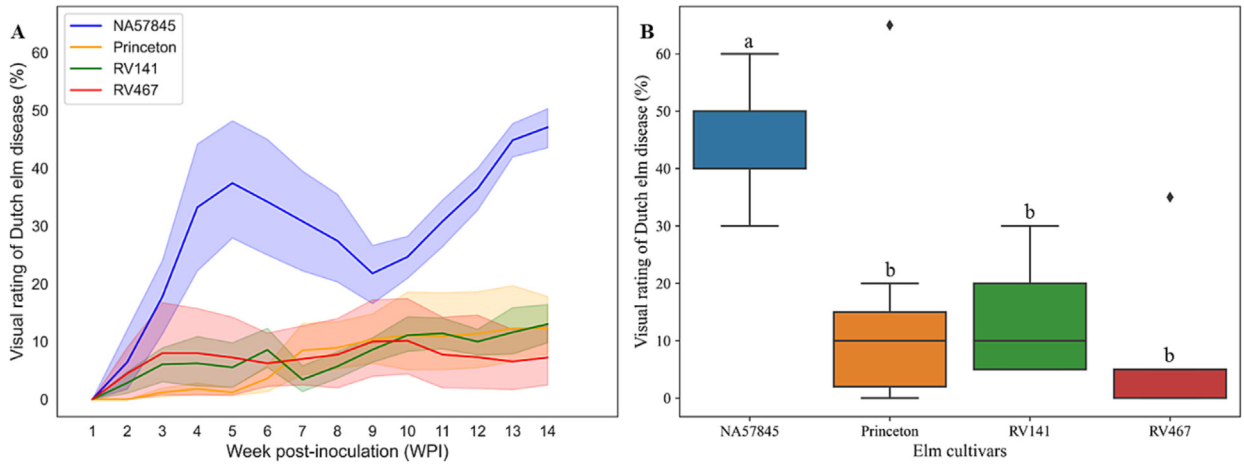

Fig. 3. (A) Disease progress curves of elm trees inoculated with *Ophiostoma novo-ulmi* based on the visual assessment foliar symptoms potentially induced by the infection of Dutch elm diseases (shaped regions were 95% confidence intervals of estimated mean of visual disease rating, $N = 4$ to 12); (B) Comparison of disease severity among four elm genotypes at 14 weeks post-inoculation using one-way Analysis of Variance (ANOVA) followed by Tukey honestly significant difference (HSD) with α level of 0.05.

symptoms among the four elm genotypes in the current study is consistent with previous studies (Flower et al., 2017; Pinchot et al., 2017), which found NA 57845 as susceptible and Princeton and RV 467 as resistant to DED. Previous studies found RV 141 to initially exhibit high tolerance to DED (Flower et al., 2017; Pinchot et al., 2017), with symptom development increasing substantially two years after inoculation (Flower, personal communication).

At 14 WPI, ~67.6% of elm trees inoculated with *O. novi-ulmi* ($N = 68$) showed foliar symptoms of DED, such as wilting, yellowing, or necrosis, and confirmed infection with DED via underbark staining. However, nearly 40% of mock-inoculated elm trees ($N = 25$) also showed some foliar symptoms, such as wilting and yellowing, but none exhibited discolorations on the xylem tissues indicating an absence of DED infection (data not shown). Foliar symptoms could be attributed to other causes besides DED, so more sensitive methods for evaluating DED are needed.

3.2. Classification performances for DED detection using hyper- and multi-spectral leaf images

Regardless of hyper- or multispectral images and machine learning methods used, overall classification accuracies varied among different sampling time points after inoculation treatments to separate leaves from mock-inoculated and inoculated elm trees. The highest classification accuracy was achieved at 15 WPI, followed by 96 HPI, and 4 WPI had the lowest classification accuracies (Table 3). The lower classification accuracy at 4 WPI than 96 HPI can be potentially explained by the second flush of vegetative growth caused by fertilizer applications after the first sampling time point at 96 HPI. The new vegetative growth might outweigh the DED infection and lead to less prominent spectral signals at 4 WPI than 96 HPI. Leaves sampled from the inoculated elm trees at 15 WPI already had visible DED symptoms, so it was expected to have a higher classification performance at 15 WPI than the first two sampling time points with no obvious foliar symptoms of DED. In addition, the temporary wet-ice storage of leaves before imaging at 96 HPI and 4 WPI might also cause leaf chemical statuses, as suggested by Juneau and Tarasoff (2012). This may potentially confound the DED signals and lead to a lower classification performance in separating leaves from mock-inoculated and inoculated elm trees at the first two sampling time points than 15 WPI (Table 3).

Generally, models built upon hyperspectral data had higher training accuracy but varied testing accuracies compared to models built upon multispectral data (averaged spectrum or cube image) (Table 3). The training accuracy represents the accuracy of a model on the data it was trained on, while the testing accuracy indicates the model's performance on unseen data. Models built upon hyperspectral data can capture fine spectral variations and potentially extract more discriminative features of leaves collected from mock-inoculated and inoculated elm trees, leading to higher training accuracy than multispectral data. However, the testing accuracies of these models can

Table 3
Classification accuracies of machine learning models for the analysis of hyper- and multi-spectral images to separate leaves from mock-inoculated and inoculated elm trees.

Models	Input	Dataset	96 HPI[f]		4 WPI[g]		15 WPI	
			Hyper[h]	Multi[i]	Hyper	Multi	Hyper	Multi
SVM[a]	Averaged spectrum[d]	Training	72.18	62.41	69.83	63.79	99.30	85.92
		Testing	62.07	62.07	56.86	43.14	90.16	75.81
PLS-DA[b]		Training	68.42	57.89	68.97	63.79	85.92	83.80
		Testing	65.52	53.45	60.78	43.14	88.52	69.35
ResNet18[c]	Cube image[e]	Training	63.36	69.17	62.61	57.14	100.00	95.00
		Testing	70.00	66.67	67.31	66.67	92.06	92.19

[a] SVM = Linear support vector machine.
[b] PLS-DA = Partial least square discriminant analysis.
[c] ResNet18 = A pretrained 18-layer deep convolutional neural network.
[d] Averaged spectrum = spectrum profile calculated by averaging all pixels of a leaf image.
[e] Cube image = three-dimensional hyper- or multispectral image cubes.
[f] HPI = hour(s) post inoculation.
[g] WPI = week(s) post inoculation.
[h] Hyper = high-spectral resolution hyperspectral LeafSpec image.
[i] Multi = high-spatial resolution multispectral LeafSpec image.

vary, indicating their sensitivity to different testing scenarios. For models built upon the averaged spectrums, hyperspectral typically had higher testing accuracies than multispectral. While for models built upon cube images, multispectral had comparable testing accuracies with hyperspectral (Table 3).

For both hyper- and multi-spectral images, deep learning models built upon cube images had higher or comparable classification accuracies in the training datasets but always higher accuracies in the testing datasets than traditional machine learning models built upon averaged spectrum (Table 3). Deep learning models, including ResNet18, often require larger amounts of training data compared to traditional machine learning models, such as SVM or PLS-DA (Zhang et al., 2020). The lower training accuracies of ResNet18 than SVM or PLS-DA could be potentially explained by the limited sample size in the current study. However, the higher testing accuracies of ResNet18 models suggest that they can effectively generalize their learned representations to distinguish between mock-inoculated and DED-inoculated treatment in unseen spectral leaf images. In addition, ResNet18 models were built directly upon spectral image cubes, which allowed them to simultaneously capture spatial and spectral features of DED infection. In contrast, SVM or PLS-DA models built upon spectrum derived from spectral images only considered spectral features, potentially missing out on valuable spatial information that can aid in accurate DED detection. Nevertheless, results indicate that the deep learning models considering both spectral and spatial features of high-resolution LeafSpec images have advantages over traditional machine learning models built upon spectral features alone for DED detection.

To better visualize leaves sampled from healthy and DED-infected elm trees, leaf-level attention maps representing spatial feature importance were generated using Grad-CAM in the ResNet18 CNN model built upon multispectral cube images. The "hotter" areas in the attention map were the prioritized locations used by the CNN model for DED detection. Two distinct feature distributions were observed between leaves from inoculated and mock-inoculated trees. Edges and symptomatic spots on the leaves were highlighted as important spatial features to distinguish leaves from inoculated and mock-inoculated trees (Fig. 4). DED infection affects the xylem water transportation, thus leading to foliar wilting symptoms (Haugen, 1998; D'Arcy, 2000; Bernier, 2022). At the leaf level, edges are away from the main xylem channel, typically major or second veins. Plants usually sacrifice leaf edges first when under vascular stress, which could explain why leaf edges were selected in addition to symptomatic spots when differentiating elm leaves from inoculated and mock-inoculated trees.

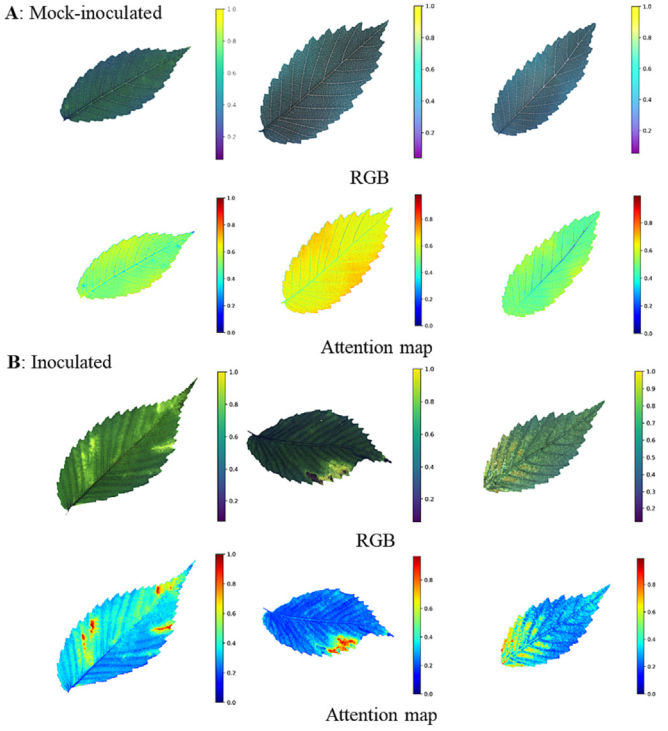

Fig. 4. RGB and attention maps of representative leaves from elm trees mock-inoculated and inoculated with *O. novo-ulmi*, the causal agent of Dutch elm disease (DED). RGB images were derived from multispectral leaf images at 15 weeks post inoculation. Attention maps representing the spatial feature patterns of the ResNet18 CNN model for DED detection were generated using Gradient-weighted Class Activation Mapping. The highlighted regions in each attention map were the most important regions in the image to predict DED infection.

3.3. Spectral and spatial feature patterns of elm genotypes with different susceptibility to DED

The best-performing DED detection models were investigated further to explore their applications in screening different elm genotypes for DED resistance. Because disease progressed differently among the four elm genotypes, classification models were built and cross-validated among elm genotypes using averaged spectrum derived from hyperspectral image cubes (Fig. 5A). Interestingly, the NA 57845 model performed better in classifying the spectrums of itself and RV 141 than the spectrums of Princeton and RV 467. These two models also had better performance in classifying the combined spectrums than Princeton and RV 467 models. On the other hand, the Princeton model performed better in classifying itself and RV 467 than classifying spectrums of NA 57845 and RV 141. These results suggest that spectral profiles of susceptible and resistant elm genotypes differ following inoculation. This may indicate differences in induced chemicals between susceptible and resistant trees following infection with *O. novo-ulmi*, as reported in previous studies (Martin et al., 2005a, 2005b, 2007, 2008).

Among the averaged spectrum models, the SVM model built upon hyperspectral images at 15 WPI had the highest prediction accuracies in distinguishing leaves from healthy and diseased elm trees. To examine which spectral wavelength(s) were most important for classification, the coefficients of the linear SVM models were plotted in Fig. 5B. Interestingly, in the visible region (e.g., ~490 to 680 nm), NA 57845 and RV 141 models had similar coefficient patterns, while Princeton and RV 467 had similar patterns. Moreover, the patterns of susceptible genotypes (NA 57845 and RV 141) differed from resistant genotypes (Princeton and RV 467). In the part of the Red-edge region (e.g. ~700 to 730 nm), RV 141 and RV 467 had similar patterns, and NA 57845 and Princeton had similar patterns. In the near-infrared region (e.g., 800 to 900 nm), the feature importance was low, as indicated by the coefficients being close to 0 (Fig. 5B). Overall, the visible region of the spectrum was important in distinguishing leaves from inoculated and mock-inoculated trees, which agreed with one previous report on spectral reflectance characteristics of DED by Wilson et al. (1998). The reflectance/transmittance at the visible region is related to leaf pigments such as chlorophyll. The wilting, yellowing, and eventually browning symptoms induced by DED might be caused by leaf pigment changes, which were captured by spectral imaging tools.

Among models directly built upon hyper- and multi-spectral image cubes, the multispectral ResNet18 model at 15 WPI had the highest prediction accuracies in distinguishing leaves from healthy and diseased elm trees. To investigate whether spatial feature patterns were useful for disease-resistant genotype screening, attention maps in the ResNet18 CNN models for DED detection were compared among the four elm genotypes evaluated in this study. Susceptible elm genotypes (NA 57845 and RV 141) had similar attention maps that differed from those of the resistant elm genotypes (Princeton and RV 467) (Fig. 6). Both the susceptible and resistant elm genotypes underwent two types of treatments: inoculated and mock-inoculated. However, when examining the attention maps, it was observed that the susceptible

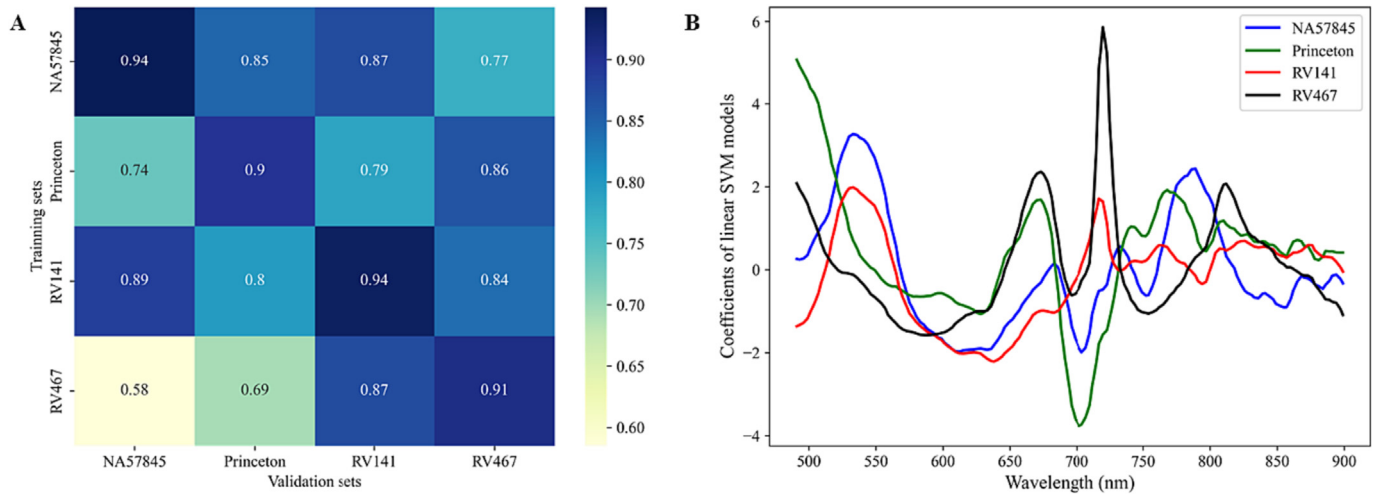

Fig. 5. (A) Classification performances of Linear Support Vector Machine (SVM) models of each elm genotype for Dutch elm disease (DED) detection via cross-validation; (B) Coefficients plots of the linear SVM models representing the importance of spectral wavelengths or features in DED classification models for each elm genotype.

elm genotypes showed attention maps with colors similar to those of the inoculated group, indicating a response to the disease. On the other hand, the attention maps of the resistant elm genotypes exhibited colors resembling those of the mock-inoculated group, suggesting a lack of response to the disease (Figs. 4 and 6). These findings provide further evidence that leaf-level spatial feature patterns identified by deep learning models can effectively distinguish between susceptible and resistant elm genotypes, which can be useful for identifying disease-resistant genotypes and informing disease management strategies.

3.4. Advantages and limitations

Two novel leaf-level imaging solutions, including high spectral resolution HSI and high spatial resolution MSI combined with machine learning, were evaluated side-by-side for the first time in detecting DED and screening genotypes for disease resistance in American elms. Results indicated that HSI had an advantage in detecting DED during the early stage of infection before disease symptoms were visible to human eyes. The rich spectral information provided by HSI could potentially capture plant early responses to the pathogen infection. Meanwhile, MSI combined with deep learning also showed an advantage in capturing symptomatic spots on the leaves once foliar disease symptoms appeared because of its high spatial resolution images. The innovative engineering design of LeafSpec, which includes an enclosed imaging chamber with embedded uniform light sources, ensured the imaging quality with a high signal-over-noise ratio and thus built a successful foundation for further machine learning-based analysis.

On the other hand, we acknowledged that the current study had some limitations. Firstly, as a proof-of-concept study, the elm trees evaluated were grown under a controlled environment. Factors like different light conditions, seasonal variations, or interactions with other pathogens might influence the spectral signatures of the leaves.

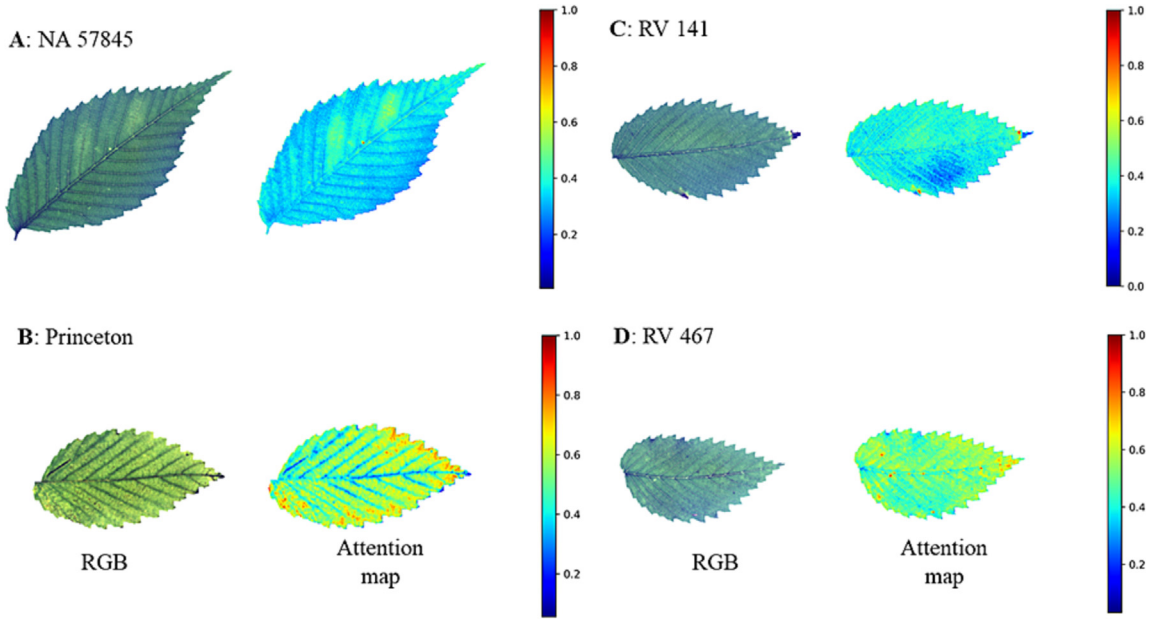

Fig. 6. RGB and attention maps of representative leaves for each elm genotype infected with Dutch elm disease (DED). RGB images were derived from multispectral leaf images at 15 weeks post inoculation. Attention maps representing the spatial feature patterns of the ResNet18 DED detection model were generated using Gradient-weighted Class Activation Mapping. The highlighted regions in each attention map were the most important regions in the image to predict DED infection.

Secondly, only four genotypes of American elms were included in this study due to logistical constraints. For future studies, it would be valuable to explore a broader range of elm genotypes to further assess the model's generalizability and validate models developed in this study under different environmental conditions, potentially enhancing its applicability. By broadening the scope of evaluated elm genotypes and testing in varied environmental settings, we believe there is immense potential to refine and extend the applicability of the proposed imaging solutions that would pave the way for advanced, accurate, and efficient DED detection and resistance screening in the future.

4. Conclusions

In the current study, high-resolution leaf images collected using both hyper and multi-spectral LeafSpec imagers combined with machine learning were able to separate leaves from DED-infected and non-infected trees, although accuracy varied depending on machine learning model and time point following inoculation. Deep learning models that incorporate both spectral and spatial features of high-resolution spectral leaf images demonstrate superior performance than traditional machine learning models built upon spectral features alone in detecting DED infection in American elm. Distinct leaf-level spatial feature distributions were also observed between elm leaves from inoculated and mock-inoculated elm trees. Similar spectral and spatial patterns were found between elm genotypes with similar susceptibility to DED after pathogen inoculation. Results demonstrate that machine learning-based spectral and spatial analysis of high-resolution hyper- and multi-spectral leaf images can detect DED and potentially be useful in screening for elm genotypes for susceptibility to DED. Though further studies are needed, these high-precision and portable spectral leaf imagers combined with machine learning have demonstrated promising potential for accurate disease phenotyping in trees.

Disclosure

N/A

CRediT authorship contribution statement

Xing Wei: Conceptualization, Methodology, Investigation, Formal analysis, Software, Visualization, Project administration, Writing - original draft. **Jinnuo Zhang**: Data curation, Formal analysis, Software, Visualization, Writing – review & editing. **Anna O. Conrad**: Conceptualization, Methodology, Writing – review & editing. **Charles E. Flower**: Conceptualization, Methodology, Resources, Writing – review & editing. **Cornelia C. Pinchot**: Conceptualization, Methodology, Resources, Writing – review & editing. **Nancy Hayes-Plazolles**: Methodology, Investigation. **Ziling Chen**: Data curation, Investigation. **Zhihang Song**: Data curation, Investigation. **Songlin Fei**: Conceptualization, Methodology, Funding acquisition, Writing – review & editing. **Jian Jin**: Conceptualization, Methodology, Funding acquisition, Resources, Writing – review & editing, Supervision.

Data availability

Data is available upon reasonable request.

Declaration of Competing Interest

The authors declare no conflicts of interest.

Acknowledgments

This work was supported in part by the United States Department of Agriculture Forest Service (USDA FS) and the Institute for Digital Forestry at Purdue University. We thank the staff and undergraduate interns with the USDA FS Northern Research Station in Delaware, OH, for the maintenance of the elm assay. We thank members of the ABE Plant Senor lab in the Department of Agricultural and Biological Engineering at Purdue University for their help with the data collection. Mention of trade names or commercial products in this article is solely for the purpose of providing specific information and does not imply recommendation or endorsement by Purdue University or USDA. Purdue and USDA are equal opportunity providers and employers.

Appendix A. Supplementary data

Supplementary data to this article can be found online at https://doi.org/10.1016/j.aiia.2023.09.003.

References

Abdulridha, J., Batuman, O., Ampatzidis, Y., 2019. UAV-based remote sensing technique to detect citrus canker disease utilizing hyperspectral imaging and machine learning. Remote Sens. 11 (11), 1373. https://doi.org/10.3390/rs11111373.

Bernier, L., 2022. Dutch elm disease. In: Asiegbu, F., Kovalchuk, A. (Eds.), Forest Microbiology. 2. Elsevier, Amsterdam, The Netherlands, pp. 291–309.

Bian, L., Zhang, H., Ge, Y., Čepl, J., Stejskal, J., El-Kassaby, Y.A., 2022. Closing the gap between phenotyping and genotyping: review of advanced, image-based phenotyping technologies in forestry. Ann. For. Sci. 79 (1), 1–21. https://doi.org/10.1186/s13595-022-01143-x.

Bock, C.H., Barbedo, J.G., Del Ponte, E.M., Bohnenkamp, D., Mahlein, A.K., 2020. From visual estimates to fully automated sensor-based measurements of plant disease severity: status and challenges for improving accuracy. Phytopathol. Res. 2 (1), 1–30. https://doi.org/10.1186/s42483-020-00049-8.

Chen, G., Meentemeyer, R.K., 2016. Remote sensing of forest damage by diseases and insects. In: Weng, Q. (Ed.), Remote Sensing for Sustainability. 2017. CRC Press, Boca Raton, FL, pp. 145–162 Section II.

Chen, Z., Wang, J., Wang, T., Song, Z., Li, Y., Huang, Y., Wang, L., Jin, J., 2021. Automated in-field leaf-level hyperspectral imaging of corn plants using a Cartesian robotic platform. Comput. Electron. Agric. 183, 105996. https://doi.org/10.1016/j.compag.2021.105996.

Chen, Z., Wang, J., Jin, J., 2023. Fully automated proximal hyperspectral imaging system for high-resolution and high-quality in vivo soybean phenotyping. Precis. Agric., 1–21 https://doi.org/10.1007/s11119-023-10045-5.

Chevallier, S., Bertrand, D., Kohler, A., Courcoux, P., 2006. Application of PLS-DA in multivariate image analysis. J. Chemom. 20 (5), 221–229. https://doi.org/10.1002/cem.994.

Conrad, A.O., Bonello, P., 2016. Application of infrared and Raman spectroscopy for the identification of disease resistant trees. Front. Plant Sci. 6, 1152. https://doi.org/10.3389/fpls.2015.01152.

Conrad, A.O., Li, W., Lee, D.Y., Wang, G.L., Rodriguez-Saona, L., Bonello, P., 2020. Machine learning-based presymptomatic detection of rice sheath blight using spectral profiles. Plant Phenomics 2020, 8954085. https://doi.org/10.34133/2020/8954085.

Cortes, C., Vapnik, V., 1995. Support-vector networks. Mach. Learn. 20, 273–297. https://doi.org/10.1007/BF00994018.

Cotrozzi, L., 2022. Spectroscopic detection of forest diseases: a review (1970–2020). J. For. Res. 33 (1), 21–38. https://doi.org/10.1007/s11676-021-01378-w.

D'Arcy, C.J., 2000. Dutch elm disease. Plant Health Instr. https://doi.org/10.1094/PHI-I-2000-0721-02 Updated 2005.

Fang, Y., Ramasamy, R.P., 2015. Current and prospective methods for plant disease detection. Biosensors 5, 537–561. https://doi.org/10.3390/bios5030537.

Fang, S., Cui, R., Wang, Y., Zhao, Y., Yu, K., Jiang, A., 2023. Application of multiple spectral systems for the tree disease detection: a review. Appl. Spectrosc. Rev. 58 (2), 83–109. https://doi.org/10.1080/05704928.2021.1930552.

Fearer, C.J., Conrad, A.O., Marra, R.E., Georskey, C., Villari, C., Slot, J., Bonello, P., 2022. A combined approach for early in-field detection of beech leaf disease using near-infrared spectroscopy and machine learning. Front. For. Glob. Change 5, 934545. https://doi.org/10.3389/ffgc.2022.934545.

Fei, S., Morin, R.S., Oswalt, C.M., Liebhold, A.M., 2019. Biomass losses resulting from insect and disease invasions in US forests. Proc. Natl. Acad. Sci. 116 (35), 17371–17376. https://doi.org/10.1073/pnas.1820601116.

Flower, C.E., Gonzalez-Meler, M.A., 2015. Responses of temperate forest productivity to insect and pathogen disturbances. Annu. Rev. Plant Biol. 66, 547–569. https://doi.org/10.1146/annurev-arplant-043014-115540.

Flower, C.E., Slavicek, J.M., Lesser, D., Eshita, S., Pinchot, C.C., 2017. Canopy decline assessments in American elm after inoculation with three doses of *Ophiostoma ulmi* and *O. novo-ulmi*. In: Pinchot, C.C., Knight, K.S., Haugen, L.M., Flower, C.E., Slavicek, J.M. (Eds.), Proceedings of the American Elm Restoration Workshop 2016; October 25-27, 2016; Lewis Center, OH. Gen. Tech. Rep. NRS-P-174. U.S. Department of Agriculture, Forest Service Northern Research Station, Newtown Square, PA, pp. 24–29.

Gitelson, A.A., Merzlyak, M.N., 1996. Signature analysis of leaf reflectance spectra: algorithm development for remote sensing of chlorophyll. J. Plant Physiol. 148 (3–4), 494–500. https://doi.org/10.1016/S0176-1617(96)80284-7.

Haugen, L., 1998. How to identify and manage Dutch elm disease. In: Ash, C.L. (Ed.), Shade Tree Wilt Diseases. APS Press, St Paul, MN, USA, pp. 37–52.

Haugen, Linda M., Bentz, Susan E., Pinchot, Cornelia C., Knight, Kathleen S., Haugen, Linda M., Flower, Charles E., Slavicek, James M., 2017. American elm clones of importance in Dutch elm disease tolerance studies. Proceedings of the American Elm Restoration Workshop 2016; 2016 October 25–27; Lewis Center, OH. Gen. Tech. Rep. NRS-P-174. U.S. Department of Agriculture, Forest Service, Northern Research Station, Newtown Square, PA, pp. 109–118.

He, K., Zhang, X., Ren, S., Sun, J., 2016. Deep residual learning for image recognition. Proceedings of the IEEE Conference on Computer Vision and Pattern Recognition, pp. 770–778.

Jiang, Y., Li, C., 2020. Convolutional neural networks for image-based high-throughput plant phenotyping: a review. Plant Phenomics 2020. https://doi.org/10.34133/2020/4152816.

Juneau, K.J., Tarasoff, C.S., 2012. Leaf area and water content changes after permanent and temporary storage. PLoS One 7 (8), e42604. https://doi.org/10.1371/journal.pone.0042604.

Kumar, A., Lee, W.S., Ehsani, R.J., Albrigo, L.G., Yang, C., Mangan, R.L., 2012. Citrus greening disease detection using aerial hyperspectral and multispectral imaging techniques. J. Appl. Remote. Sens. 6 (1), 063542. https://doi.org/10.1117/1.JRS.6.063542.

Li, X., Chen, Z., Wang, J., Jin, J., 2023a. LeafSpec-dicot: an accurate and portable hyperspectral imaging device for dicot leaves. Sensors 23 (7), 3687. https://doi.org/10.3390/s23073687.

Li, X., Chen, Z., Wei, X., Zhao, T., Jin, J., 2023b. Development of a target-to-sensor mode multispectral imaging device for high-throughput and high-precision touch-based leaf-scale soybean phenotyping. Sensors 23 (7), 3756. https://doi.org/10.3390/s23073756.

Liu, J., Wang, X., 2021. Plant diseases and pests detection based on deep learning: a review. Plant Methods 17, 1–18. https://doi.org/10.1186/s13007-021-00722-9.

Ma, D., Wang, L., Zhang, L., Song, Z.U., Rehman, T., Jin, J., 2020. Stress distribution analysis on hyperspectral corn leaf images for improved phenotyping quality. Sensors 20 (13), 3659. https://doi.org/10.3390/s20133659.

Ma, D., Rehman, T.U., Zhang, L., Maki, H., Tuinstra, M.R., Jin, J., 2021. Modeling of environmental impacts on aerial hyperspectral images for corn plant phenotyping. Remote Sens. 13 (13), 2520. https://doi.org/10.3390/rs13132520.

Martin, J.A., Solla, A., Coimbra, M.A., Gil, L., 2005a. Metabolic distinction of *Ulmus minor* xylem tissues after inoculation with *Ophiostoma novo-ulmi*. Phytochemistry 66, 2458–2467. https://doi.org/10.1016/j.phytochem.2005.08.004.

Martin, J.A., Solla, A., Woodward, S., Gil, L., 2005b. Fourier transform-infrared spectroscopy as a new method for evaluating host resistance in the Dutch elm disease complex. Tree Physiol. 25, 1331–1338. https://doi.org/10.1093/treephys/25.10.1331.

Martin, J.A., Solla, A., Woodward, S., Gil, L., 2007. Detection of differential changes in lignin composition of elm xylem tissues inoculated with *Ophiostoma novo-ulmi* using Fourier transform-infrared spectroscopy. For. Pathol. 37, 187–191. https://doi.org/10.1111/j.1439-0329.2007.00495.x.

Martin, J.A., Solla, A., Coimbra, M.A., Gil, L., 2008. Metabolic fingerprinting allows discrimination between *Ulmus pumila* and *U. minor*, and between *U. minor* clones of different susceptibility to Dutch elm disease. For. Pathol. 38, 244–256. https://doi.org/10.1111/j.1439-0329.2007.00542.x.

Mishra, P., Asaari, M.S.M., Herrero-Langreo, A., Lohumi, S., Diezma, B., Scheunders, P., 2017. Close range hyperspectral imaging of plants: a review. Biosyst. Eng. 164, 49–67. https://doi.org/10.1016/j.biosystemseng.2017.09.009.

Mishra, P., Polder, G., Vilfan, N., 2020. Close range spectral imaging for disease detection in plants using autonomous platforms: a review on recent studies. Curr. Robot. Rep. 1, 43–48. https://doi.org/10.1007/s43154-020-00004-7.

Paszke, A., Gross, S., Massa, F., Lerer, A., Bradbury, J., Chanan, G., Killeen, T., Lin, Z., Gimelshein, N., Antiga, L., Desmaison, A., Kopf, A., Yang, E., DeVito, Z., Raison, M., Tejani, A., Chilamkurthy, S., Steiner, B., Fang, L., Bai, J., Chintala, S., 2019. Pytorch: an imperative style, high-performance deep learning library. Adv. Neural Inf. Proces. Syst. 32.

Pedregosa, F., Varoquaux, G., Gramfort, A., Michel, V., Thirion, B., Grisel, O., Blondel, M., Prettenhofer, P., Weiss, R., Dubourg, V., 2011. Scikit-learn: machine learning in Python. J. Mach. Learn. Res. 12, 2825–2830.

Peng, Y., Dallas, M.M., Ascencio-Ibáñez, J.T., Hoyer, J.S., Legg, J., Hanley-Bowdoin, L., Grieve, B., Yin, H., 2022. Early detection of plant virus infection using multispectral imaging and spatial–spectral machine learning. Sci. Rep. 12 (1), 3113. https://doi.org/10.1038/s41598-022-06372-8.

Pinchot, C.C., Flower, C.E., Knight, K.S., Marks, C., Minocha, R., Lesser, D., Woeste, K., Schaberg, P.G., Baldwin, B., Delatte, D.M., Fox, T.D., Hayes-plazolle, N., Held, B., Lehtoma, K., Long, S., Mattix, S., Sipes, A., Slavicek, J.M., Sniezko, Richard A., Man, Gary, Hipkins, Valerie, Woeste, Keith, 2017. Development of new Dutch elm disease-tolerant selections for restoration of the American elm in urban and forested landscapes. Proceedings of Workshop on Gene Conservation of Tree Species-Banking on the Future. May 16-19, 2016; Chicago, IL, pp. 53–63.

Schaad, N.W., Frederick, R.D., 2002. Real-time PCR and its application for rapid plant disease diagnostics. Can. J. Plant Pathol. 24, 250–258. https://doi.org/10.1080/07060660209507006.

Selvaraju, R.R., Cogswell, M., Das, A., Vedantam, R., Parikh, D., Batra, D., 2017. Grad-cam: visual explanations from deep networks via gradient-based localization. Proceedings of the IEEE International Conference on Computer Vision, pp. 618–626.

Shi, T., Liu, Y., Zheng, X., Hu, K., Huang, H., Liu, H., Huang, H., 2023. Recent advances in plant disease severity assessment using convolutional neural networks. Sci. Rep. 13 (1), 2336. https://doi.org/10.1038/s41598-023-29230-7.

Singh, V., Sharma, N., Singh, S., 2020. A review of imaging techniques for plant disease detection. Artif. Intell. Agric. 4, 229–242. https://doi.org/10.1016/j.aiia.2020.10.002.

Song, Z., Wei, X., Jin, J., 2023. NLCS-A novel coordinate system for spatial analysis on hyperspectral leaf images and an improved nitrogen index for soybean plants. Comput. Electron. Agric. 204, 107550. https://doi.org/10.1016/j.compag.2022.107550.

Townsend, A.M., Bentz, S.E., Douglass, L.W., 2005. Evaluation of 19 American elm clones for tolerance to Dutch elm disease. J. Environ. Hortic. 23, 21–24. https://doi.org/10.24266/0738-2898-23.1.21.

Wang, L., Jin, J., Song, Z., Wang, J., Zhang, L., Rehman, T.U., Ma, D., Carpenter, N.R., Tuinstra, M.R., 2020a. LeafSpec: an accurate and portable hyperspectral corn leaf imager. Comput. Electron. Agric. 169, 105209. https://doi.org/10.1016/j.compag.2019.105209.

Wang, L., Duan, Y., Zhang, L., Wang, J., Li, Y., Jin, J., 2020b. LeafScope: a portable high-resolution multispectral imager for in vivo imaging soybean leaf. Sensors 20 (8), 2194. https://doi.org/10.3390/s20082194.

Wei, X., Johnson, M.A., Langston Jr., D.B., Mehl, H.L., Li, S., 2021a. Identifying optimal wavelengths as disease signatures using hyperspectral sensor and machine learning. Remote Sens. 13 (14), 2833. https://doi.org/10.3390/rs13142833.

Wei, X., Aguilera, M., Walcheck, R., Tholl, D., Li, S., Langston Jr., D.B., Mehl, H.L., 2021b. Detection of soilborne disease utilizing sensor technologies: lessons learned from studies on stem rot of peanut. Plant Health Prog. 22 (4), 436–444. https://doi.org/10.1094/PHP-03-21-0055-SYN.

Wilson, B.A., Luther, J.E., Stuart, T.D.T., 1998. Spectral reflectance characteristics of Dutch elm disease. Can. J. Remote. Sens. 24 (2), 200–205. https://doi.org/10.1080/07038992.1998.10855239.

Zhang, L., Maki, H., Ma, D., Sánchez-Gallego, J.A., Mickelbart, M.V., Wang, L., Rehman, T.U., Jin, J., 2019a. Optimized angles of the swing hyperspectral imaging system for single corn plant. Comput. Electron. Agric. 156, 349–359. https://doi.org/10.1016/j.compag.2018.11.030.

Zhang, L., Wang, L., Wang, J., Song, Z., Rehman, T.U., Bureetes, T., Ma, D., Chen, Z., Neeno, S., Jin, J., 2019b. Leaf scanner: a portable and low-cost multispectral corn leaf scanning device for precise phenotyping. Comput. Electron. Agric. 167, 105069. https://doi.org/10.1016/j.compag.2019.105069.

Zhang, J., Yang, Y., Feng, X., Xu, H., Chen, J., He, Y., 2020. Identification of bacterial blight resistant rice seeds using terahertz imaging and hyperspectral imaging combined with convolutional neural network. Front. Plant Sci. 11, 821. https://doi.org/10.3389/fpls.2020.00821.